Miniaturized high-NA focusing-mirror multiple optical tweezers

Fabrice Merenda, Johann Rohner, Jean-Marc Fournier and René-Paul Salathé
Advanced Photonics Laboratory
École Polytechnique Fédérale de Lausanne, Station 17, CH-1015 Lausanne, Switzerland
fabrice.merenda@epfl.ch

Abstract: An array of high numerical aperture parabolic micromirrors ($NA = 0.96$) is used to generate multiple optical tweezers and to trap micron-sized dielectric particles in three dimensions within a fluidic device. The array of micromirrors allows generating arbitrarily large numbers of 3D traps, since the whole trapping area is not restricted by the field-of-view of the high-NA microscope objectives used in traditional tweezers arrangements. Trapping efficiencies of $Q_r^{max} \simeq 0.22$, comparable to those of conventional tweezers, have been measured. Moreover, individual fluorescence light from all the trapped particles can be collected simultaneously with the high-NA of the micromirrors. This is demonstrated experimentally by capturing more than 100 fluorescent micro-beads in a fluidic environment. Micromirrors may easily be integrated in microfluidic devices, offering a simple and very efficient solution for miniaturized optical traps in lab-on-a-chip devices.

OCIS codes: (140.7010) Trapping; (170.4520) Optical confinement and manipulation; (350.3950) Micro-optics; (170.4520) Cell analysis; (040.1240) Arrays; (999.9999) Microfluidics; Lab-on-a-chip

References and links

1. A. Ashkin, "Acceleration and Trapping of Particles by Radiation Pressure," Phys. Rev. Lett. **24**, 156 (1970).
2. A. Ashkin, J. M. Dziedzic, J. E. Bjorkholm, and S. Chu, "Observation of a Single-Beam Gradient Force Optical Trap for Dielectric Particles," Opt. Lett. **11**, 288–290 (1986).
3. D. R. Reyes, D. Iossifidis, P. A. Auroux, and A. Manz, "Micro total analysis systems. 1. Introduction, theory, and technology," Anal. Chem. **74**, 2623–2636 (2002).
4. F. Arai, A. Ichikawa, M. Ogawa, T. Fukuda, K. Horio, and K. Itoigawa, "High-speed separation system of randomly suspended single living cells by laser trap and dielectrophoresis," Electrophoresis **22**, 283–288 (2001).
5. J. Enger, M. Goksor, K. Ramser, P. Hagberg, and D. Hanstorp, "Optical tweezers applied to a microfluidic system," Lab. Chip **4**, 196–200 (2004).
6. M. P. MacDonald, G. C. Spalding, and K. Dholakia, "Microfluidic sorting in an optical lattice," Nature **426**, 421–424 (2003).
7. M. M. Wang, E. Tu, D. E. Raymond, J. M. Yang, H. C. Zhang, N. Hagen, B. Dees, E. M. Mercer, A. H. Forster, I. Kariv, P. J. Marchand, and W. F. Butler, "Microfluidic sorting of mammalian cells by optical force switching," Nat. Biotechnol. **23**, 83–87 (2005).
8. S. Gaugiran, S. Getin, J. M. Fedeli, G. Colas, A. Fuchs, F. Chatelain, and J. Derouard, "Optical manipulation of microparticles and cells on silicon nitride waveguides," Opt. Express **13**, 6956–6963 (2005).
9. J. M. Fournier, M. M. Burns, and J. A. Golovchenko, "Writing Diffractive Structures by Optical Trapping," in *Practical Holography IX*, S. A. Benton, eds., Proc. SPIE **2406**, pp. 101–111 (1995).
10. E. R. Dufresne and D. G. Grier, "Optical tweezer arrays and optical substrates created with diffractive optics," Rev. Sci. Instrum. **69**, 1974–1977 (1998).

#80805 - $15.00 USD Received 8 Mar 2007; revised 25 Apr 2007; accepted 27 Apr 2007; published 2 May 2007

11. J. Rohner, J. M. Fournier, P. Jacquot, F. Merenda, and R. P. Salathe, "Multiple optical trapping in high gradient interference fringes," in *Optical Trapping and Optical Micromanipulation III*, K. Dholakia and G. C. Spalding, eds., Proc. SPIE **6326**, 6326-07 (2006).
12. C. D. Mellor and C. D. Bain, "Array formation in evanescent waves," Chemphyschem **7**, 329–332 (2006).
13. Y. Ogura, K. Kagawa, and J. Tanida, "Optical manipulation of microscopic objects by means of vertical-cavity surface-emitting laser array sources," Appl. Opt. **40**, 5430–5435 (2001).
14. C. H. Sow, A. A. Bettiol, Y. Y. G. Lee, F. C. Cheong, C. T. Lim, and F. Watt, "Multiple-spot optical tweezers created with microlens arrays fabricated by proton beam writing," Appl. Phys. B **78**, 705–709 (2004).
15. J. M. Tam, I. Biran, and D. R. Walt, "An imaging fiber-based optical tweezer array for microparticle array assembly," Appl. Phys. Lett. **84**, 4289–4291 (2004).
16. K. Sasaki, M. Koshioka, H. Misawa, N. Kitamura, and H. Masuhara, "Pattern-Formation and Flow-Control of Fine Particles by Laser-Scanning Micromanipulation," Opt. Lett. **16**, 1463–1465 (1991).
17. M. Reicherter, T. Haist, E. U. Wagemann, and H. J. Tiziani, "Optical particle trapping with computer-generated holograms written on a liquid-crystal display," Opt. Lett. **24**, 608–610 (1999).
18. R. L. Eriksen, P. C. Mogensen, and J. Gluckstad, "Multiple-beam optical tweezers generated by the generalized phase-contrast method," Opt. Lett. **27**, 267–269 (2002).
19. A. Constable, J. Kim, J. Mervis, F. Zarinetchi, and M. Prentiss, "Demonstration of a Fiberoptic Light-Force Trap," Opt. Lett. **18**, 1867–1869 (1993).
20. S. J. Cran-McGreehin, K. Dholakia, and T. F. Krauss, "Monolithic integration of microfluidic channels and semiconductor lasers," Opt. Express **14**, 7723–7729 (2006).
21. Z. H. Liu, C. K. Guo, J. Yang, and L. B. Yuan, "Tapered fiber optical tweezers for microscopic particle trapping: fabrication and application," Opt. Express **14**, 12,510–12,516 (2006).
22. H. Ottevaere, R. Cox, H. P. Herzig, T. Miyashita, K. Naessens, M. Taghizadeh, R. Volkel, H. J. Woo, and H. Thienpont, "Comparing glass and plastic refractive microlenses fabricated with different technologies," J. Opt. A-Pure Appl. Op. **8**, S407–S429 (2006).
23. K. B. Im, H. I. Kim, I. J. Joo, C. H. Oh, S. H. Song, P. S. Kim, and B. C. Park, "Optical trapping forces by a focused beam through two media with different refractive indices," Opt. Commun. **226**, 25–31 (2003).
24. P. Nussbaum, R. Volke, H. P. Herzig, M. Eisner, and S. Haselbeck, "Design, fabrication and testing of microlens arrays for sensors and microsystems," Pure Appl. Opt. **6**, 617–636 (1997).
25. A. Ashkin, "Forces of a Single-Beam Gradient Laser Trap on a Dielectric Sphere in the Ray Optics Regime," Biophys. J. **61**, 569–582 (1992).
26. S. Wakiya, "Viscous Flows Past a Spheroid," J. Phys. Soc. Jpn **12**, 1130–1141 (1957).
27. M. Lieb and A. Meixner, "A high numerical aperture parabolic mirror as imaging device for confocal microscopy," Opt. Express **8**, 458–474 (2001).
28. N. B. Simpson, D. McGloin, K. Dholakia, L. Allen, and M. J. Padgett, "Optical tweezers with increased axial trapping efficiency," J. Mod. Opt. **45**, 1943–1949 (1998).
29. A. T. O'Neill and M. J. Padgett, "Axial and lateral trapping efficiency of Laguerre-Gaussian modes in inverted optical tweezers," Opt. Commun. **193**, 45–50 (2001).
30. F. Merenda, G. Boer, J. Rohner, G. Delacretaz, and R. P. Salathe, "Escape trajectories of single-beam optically trapped micro-particles in a transverse fluid flow," Opt. Express **14**, 1685–1699 (2006).
31. W. H. Wright, G. J. Sonek, and M. W. Berns, "Parametric Study of the Forces on Microspheres Held by Optical Tweezers," Appl. Opt. **33**, 1735–1748 (1994).
32. C. G. Xie, M. A. Dinno, and Y. Q. Li, "Near-infrared Raman spectroscopy of single optically trapped biological cells," Opt. Lett. **27**, 249–251 (2002).
33. J. C. Roulet, R. Volkel, H. P. Herzig, E. Verpoorte, N. F. de Rooij, and R. Dandliker, "Fabrication of multilayer systems combining microfluidic and microoptical elements for fluorescence detection," J. Microelectromech. Syst. **10**, 482–491 (2001).

1. Introduction

In 1970, Arthur Ashkin demonstrated how milliwatts of laser radiation can be used to accelerate end even trap micron-sized particles suspended in liquid and gas [1] and in 1986 he demonstrated the single-beam gradient force optical trap, commonly referred to as *optical tweezers* [2]. Today, much interest is given to explore possibilities for combining optical forces with microfluidic systems (lab-on-a-chip or miniaturized analysis systems [3]). Optical forces have been proposed for trapping and manipulating [4, 5], sorting [6, 7] or guiding [8] micron-sized artificial as well as biological particles within microfluidic devices, demonstrating the potential of this micro-manipulation technique for future miniaturized analysis systems.

Integrating large matrices of optical traps in microfluidic devices may allow performing par-

#80805 - $15.00 USD Received 8 Mar 2007; revised 25 Apr 2007; accepted 27 Apr 2007; published 2 May 2007

allel and well controlled bio-chemical reactions on arrays of mesoscopic objects, including living cells, for the assessment of statistical data, drug screening, or for recovery of rare primary cells. Several multiple optical trapping schemes have already been proposed relying on very different techniques, including diffractive elements [9, 10], interfering beams [11, 12], VCSEL arrays [13], microlens arrays [14] or optical fiber-bundles [15]. Certain optical trapping schemes even allow generating multiple traps that are computer-reconfigurable using laser scanning [16] or spatial light modulators [17, 18].

However, the miniaturization has essentially been restricted to the microfluidic side. Today's optical trapping schemes mostly rely on macroscopic optical components and on rather complex, cumbersome optical set-ups, commonly arranged around fluorescence microscopes. Also, the very limited field-of-view of high numerical aperture objective lenses commonly employed for optical trapping realistically restricts the number of particles that can be trapped simultaneously, especially if such particles have relatively large dimensions, as it is the case for living cells. The miniaturization of the optical components needed for optical trapping could lead to innovative optical trapping and analysis systems, partially or completely integrating optics and microfluidics within the same analysis biochip. A miniaturized version of the counter-propagating two-beam trap was achieved in the 90's using two facing optical fibers [19]. This trapping configuration was recently demonstrated in a completely miniaturized device embedding both the trapping laser sources and the microfluidics within the same monolithic semiconductor [20]. Miniaturizing the single-beam gradient force optical trap would require high numerical aperture (NA) micro-optical components, which is hardly attainable. The only successful example so far has taken advantage of a special tapered optical fiber [21].

In this article we demonstrate that miniaturized focusing mirrors can provide the high-NA necessary for generating single-beam optical traps with micro-optical components. Furthermore, arrays of such micromirrors provide a highly scalable approach for generating a large number of optical traps, and may be directly integrated into microfluidic devices.

2. Parabolic micromirrors as high-NA micro-optics

When operating in a single-beam configuration, optical traps rely on highly convergent light beams (at least $NA > 0.7$, but typically $NA > 1$) capable of trapping micrometer-sized dielectric particles in three dimensions. Typically, objective lenses are employed to perform such a tight focusing task. Although single aspheric air-immersed lenses with NAs as high as 0.7 are commercially available, such a high NA can hardly be reached with microlenses [22]. Simple calculations show that the sides of a single-sided aspherical microlens should be very steep relative to the substrate if standard optical glass ($n \simeq 1.56$) is used. High-index materials, such as silicon, are not employable in the visible and near-infrared ranges due to their poor optical transmission at these wavelengths. Besides the technical issues related to the fabrication of high-aspect ratio aspherical microlenses, their effective numerical aperture is limited because the high incidence angles strongly restrict the fraction of light which is effectively refracted at the higher NAs. Graded-index (GRIN) lens arrays might also be considered, but their NA is usually limited to 0.5, which is insufficient to generate single-beam optical traps. Special GRIN fiber bundles with NA as high as 1.0 have been used for multiple optical trapping [15], but for some unspecified reason 3D optical trapping could not be achieved. Hybrid approaches, e.g. plano-convex microlenses featuring a refractive index increase towards the side of the lens may provide an opportunity to reach higher NAs, but do not seem to be technically feasible at this time.

Instead, a parabolic mirror directly allows for high-NA light focusing, and it is also well suited for miniaturization. Fig. 1(a) illustrates the parabolic mirror basic focusing geometry and main parameters: diameter d and paraxial radius of curvature R. A parallel beam, travelling

#80805 - $15.00 USD Received 8 Mar 2007; revised 25 Apr 2007; accepted 27 Apr 2007; published 2 May 2007

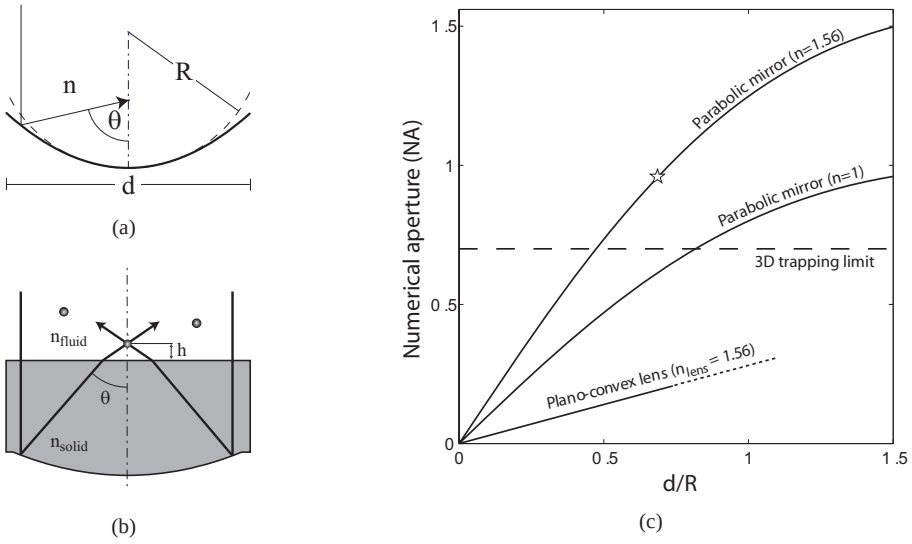

Fig. 1. (a) Mirror parameters and basic focusing geometry. (b) Geometry of the focusing mirrors used in the described experiments. The reflection on the mirror takes place within a solid media of refractive index n_{solid}, allowing a higher NA to be generated (c) Numerical aperture achievable with parabolic mirrors, both considering reflection in air ($n = 1$) or in a higher refractive index solid ($n = 1.56$), compared to that of a single plano-convex lens (lower straight line, paraxial approximaton), as a function of the diameter d to radius-of-curvature R ratio. The star ($\star$) indicates the aperture achieved in the present work.

along the mirror optical axis, is focused to one point without aberrations in the geometrical approximation. The numerical aperture of a parabolic mirror (PM) is given by

$$NA_{PM} = n\sin\left[2\arctan\left(\frac{d}{2R}\right)\right] \tag{1}$$

where n is the refractive index of the media immediately adjacent to the mirror's reflecting surface. As it will be described in the next section, we have produced focusing parabolic micromirrors by negative replication of an array of plano-convex microlenses. A comparison between the NAs of the master microlenses with that achievable with the molded micromirrors is implemented in Fig. 1(c). Both the lenses and the mirrors are characterized by the same diameter to radius-of-curvature ratio d/R. For the plano-convex lens, we assume a paraxial approximation

$$NA_L \simeq (n_{lens} - 1)\frac{d}{2R} \tag{2}$$

and consider that the lens is composed of conventional optical glass with index of refraction $n_{lens} = 1.56$. This paraxial approximation (straight line ending in dots) is reasonable at least for plano-convex lenses characterized by apertures up to $NA_L \simeq 0.2$. In the very low-NA limit ($d/R << 1$), a paraxial approximation may also be considered for the mirrors ($NA_{PM} \simeq nd/R$). Within this limit, the NA of an air-immersed ($n = 1$) parabolic mirror is more than three times higher than the one of a single plano-convex lens having the same diameter and radius of curvature

$$\frac{NA_{PM}}{NA_L} \simeq 3.57n, \quad d/R << 1 \tag{3}$$

#80805 - $15.00 USD Received 8 Mar 2007; revised 25 Apr 2007; accepted 27 Apr 2007; published 2 May 2007

The factor n in Eq. (3) appears because the angles θ at which rays are redirected by the mirror are independent of the adjacent media's refractive index, conversely to the refraction at a lens curved interface. Therefore, if the media on the reflection side of the mirror is characterized by an index of refraction n higher than unity, the NA of the mirror is even further increased by a factor n. The example reported in Fig. 1(c) assumes that the mirror is immersed in a dielectric media characterized by the same refractive index as the one of the lens ($n = n_{lens} = 1.56$). This corresponds to a ratio NA_{PM}/NA_L of 5.57 in the paraxial limit. In the non-paraxial regime, this ratio is somewhat reduced due to the non-linearity of Eq. (1), but still is close to five in practical cases.

The particular physical configuration of the parabolic mirrors used in the present experiments is illustrated in Fig. 1(b). The volume on the concave side of the mirror, where reflection takes place, is filled by a solid characterized by a high index of refraction n_{solid}. The focus of the mirror is located within the adjacent fluid containing particles to be trapped (typically water) which has an index of refraction n_{fluid}, lower than the one of the embedding media n_{solid}. The NA gain factor with respect to a mirror that would be filled by the fluid still is of n_{solid}/n_{fluid}. Some spherical aberration is introduced in the system (similarly as with oil-immersion microscope objectives) but a resulting reduction in the trapping efficiency is expected to be limited provided that the distance h between the interface and the foci is kept small [23].

As shown in Fig. 1(c), micromirrors are easily overcoming the NA requirements for 3D trapping ($NA > 0.7$, horizontal dashed line). This limit is indicative, since it depends on the characteristics of the object to be trapped. The star ($\star$) indicates the aperture achieved by the micromirrors produced in the framework of this work. Their fabrication is described in the next section.

3. Experimental

3.1. Micro-mirror array fabrication

An array of parabolic micro-mirrors was successfully produced by molding in UV-curing resist a commercially available array of micro-lenses (Süss MicroOptics, Neuchâtel, Switzerland). These fused silica microlenses ($NA = 0.15$) have a diameter of $240\mu m$, a radius of curvature of $350\mu m$. Their crucial characteristic for this project is the aspherical cross-sectional profile characterized by a conic constant of $K = -1$, corresponding to a parabola [24]. The microlenses are arranged on a hexagonal array with a pitch of $250\mu m$, the $5mm \times 5mm$ array containing more than 400 microlenses.

As illustrated in Fig. 2, a thin gold layer ($60nm$) is evaporated onto the microlens array prior to the replication of the surface relief into a UV-curing resist (Norland optical adhesive 81, $n = 1.56$) on a $1mm$ thick microscope slide. After polymerization and removal of excessive resist, the microlens array is detached from the microscope slide. The low adhesion of gold to the silica of the microlenses - as compared to its adhesion to the hardened resist - ensures that the gold composing the reflective surface of the micromirrors is transferred to the resist side. A second layer of the same UV-curing resist is applied onto the micro-mirrors, and a $80\mu m$ thick cover-glass (Menzel #00) is deposited on top prior to a second curing step.

The very thin gold layer ensures that the mirrors are partially transparent to visible light, but highly reflective to the near infrared trapping wavelength (98.6% reflectivity calculated at $1064nm$, the rest being essentially absorbed in the gold layer). In addition to the gain in NA with respect to a water-immersed mirror, there are several other reasons why the micromirror array is merged in resist and covered by a thin glass. The first, most important objective, is allowing the foci to be located a few microns above the cover-glass, which will constitute the bottom of a fluidic channel. This ensures that the particles in the channel will flow in the vicinity of the foci and will be captured efficiently. Second, since the refractive index is the same on both sides of

#80805 - $15.00 USD Received 8 Mar 2007; revised 25 Apr 2007; accepted 27 Apr 2007; published 2 May 2007

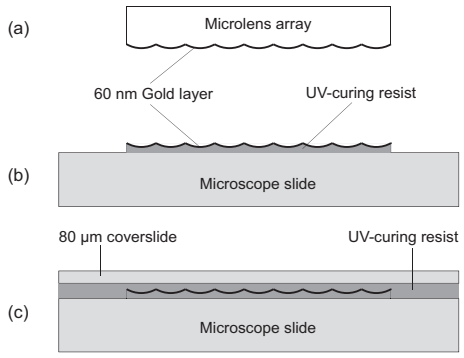

Fig. 2. Fabrication of the micromirror array: (a) 60 nm of gold are evaporated on an array of parabolic microlenses (b) Negative replication in UV-curing resist forms the focusing micromirror array. The thin gold layer detaches from the microlens array, forming the reflective surface on the hardened resist (c) A 80 μm thick cover-glass is glued on top with additional resist merging the micromirrors.

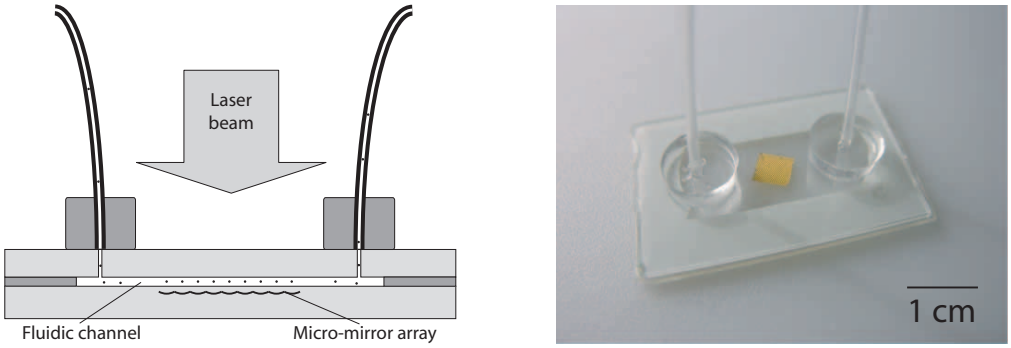

(a) (b)

Fig. 3. (a) Schematic illustration of the assembled fluidic device. The solution of particles flows between two microscope slides: the bottom microscope slide embedding the micromirror array and the top microscope slide with holes for fluidic access. Simply directing a collimated laser beam on the fluidic device creates the traps in the fluidic channel. (b) Picture of the assembled fluidic device. The array of golden micromirrors can be seen in the center.

the mirrors, the micromirror array does not act as a diverging microlens array when observing in transmission using visible light, allowing undisturbed imaging of the trapping area. Finally, the delicate resist structure composing the micromirrors is mechanically stabilized and the gold layer is well protected; this permits easy cleaning and re-use of the device.

The microlenses that were used as a master mold for the mirrors are made of fused silica, which has a relatively low index refractive index ($n_{lens} = 1.45$ at $1064nm$). As a consequence, they are characterized by a relatively low NA of 0.15, and in this particular case the ratio NA_{PM}/NA_L is as high as six. The resist-immersed parabolic mirrors reach an aperture of $NA = 0.96$.

3.2. Fluidic device

The fluidic device developed for the purpose of testing the micro-mirror traps is illustrated in Fig. 3. Its bottom is composed of the microscope slide of Fig. 2(c) with embedded micromir-

#80805 - $15.00 USD Received 8 Mar 2007; revised 25 Apr 2007; accepted 27 Apr 2007; published 2 May 2007

rors. Two holes are drilled into a second $1mm$ thick microscope slide, on top of which two PDMS-elastomer pieces providing support for the fluid access tubings are bonded by surface activation in a mild oxygen-plasma discharge. A $100\mu m$ thick two-sided adhesive tape, cut-up in its center to form the main fluidic channel, bonds the two microscope slides and provides a seal for the solution to be flown in the system. Two $1ml$ microcentrifuge tubes are used as reservoirs and connected by plastic tubes to the fluidic system (omitted in Fig. 3). The input and output reservoirs are positioned respectively a few centimeters below and above the fluidic chamber. Smooth fluid flow is generated with little air pressure (fraction of a *mbar*) applied to the input reservoir and controlled by a manual pressure regulator. Reducing the pressure generates backward flow thanks to a communicating vessel mechanism. The traps in the channel are simply generated by directing a collimated laser beam onto the fluidic device (the micromirrors being embedded in the device).

3.3. Laser sources, observation and fluorescence detection

The optical set-up employed in the present experiments is schematically illustrated in Fig. 4. The trapping laser source is an Ytterbium fiber laser (IPG Photonics) emitting in a linearly polarized TEM_{00} mode at a wavelength of $1064nm$ and delivering up to $10W$ adjustable optical power. Two fluorescence excitation He-Ne laser beams (Polytech GmBh $543nm/0.5mW$, $633nm/2mW$) are expanded to a diameter close to that of the trapping laser (roughly $5mm$ for a $1/e^2$ irradiance drop) and coupled in the trapping laser path using a lowpass filter. The three laser beams strike upon the micromirror array at perpendicular incidence and are focused confocally by the micromirrors.

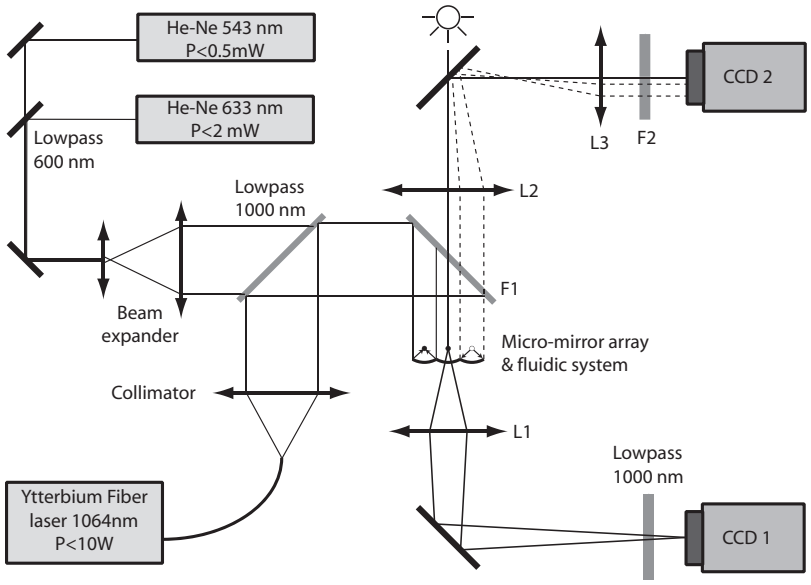

Fig. 4. Optical set-up. *Left*: lasers for trapping and for fluorescence excitation. *Right-above*: fluorescence signals detection. The light emitted by the particles is collected at high-NA by the micromirrors and relayed onto CCD2 trough a $4f$ system. F1 and F2 are custom designed filters being highly reflective for the trapping laser and fluorescence excitation laser wavelengths, but transmissive for emitted fluorescence. *Right-below*: observation is performed in transmission through micromirror array partially transparent to visible light.

Observation of the trapping area with CCD1 is achieved in transmission across the micromir-

#80805 - $15.00 USD Received 8 Mar 2007; revised 25 Apr 2007; accepted 27 Apr 2007; published 2 May 2007

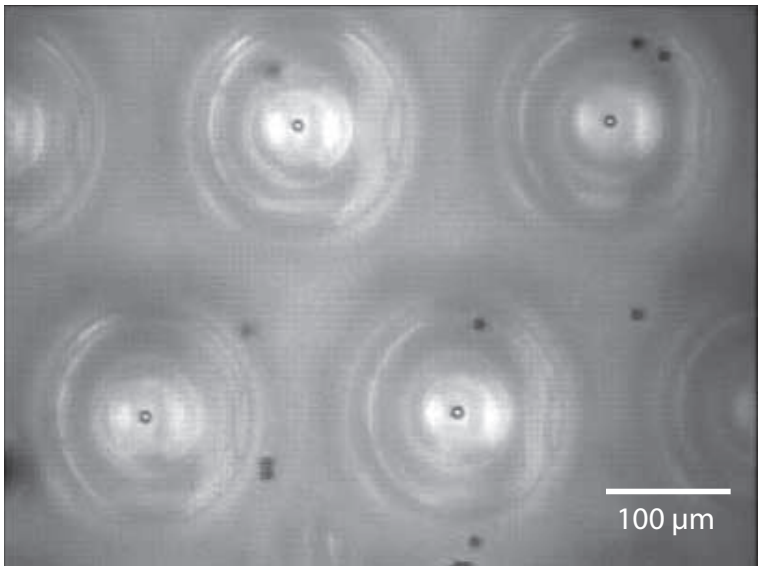

Fig. 5. (Movie 2.43MB) Transmission image ($10\times$) of four $9.33\mu m$ diameter polystyrene beads trapped in three dimensions at the focus of the parabolic micromirrors. The movie shows real time trapping both at $10\times$ and $5\times$ magnifications, and escape velocity measurements.

ror array, being partially transparent to visible light, with different magnifications ($L1$).

In addition to providing the high-NA necessary for 3D optical trapping, the micromirrors are also used to collect fluorescence light emitted by the particles. Indeed, since particles are trapped at the focus of the mirrors, emitted fluorescence light is collected with high efficiency by the mirrors and quasi-collimated beams are subsequently relayed on a color camera (CCD2, PCO Pixelfly) through a $4f$ relay telescope system ($0.8\times$) composed of lenses $L2$ and $L3$. $F1$ and $F2$ are custom designed filters (Chroma) being highly reflective at the wavelengths of the trapping laser and the fluorescence excitation lasers, but highly transmissive in passbands for fluorescence emission wavelengths.

4. Results

4.1. 3D trapping

Several solutions of polystyrene beads, with diameters ranging from 2.5 to 15 μm, were introduced in the fluidic system to test optical trapping with the micromirrors. All sizes could successfully be trapped in three dimensions. Figure 5 illustrates a transmission image of four $9.33\mu m$ polystyrene beads (Polysciences, Inc.) trapped at the focus of the parabolic micromirrors. Several arguments demonstrate that 3D trapping is achieved in the present experiments. By subsequently imaging the trapped particles and particles deposited at the bottom of the fluidic channel, the trapping plane was estimated to lie about $20\mu m$ inside the channel. Since the total depth of the channel approximates $100\mu m$, particles certainly are not pushed against the ceiling of the channel. Another evidence demonstrating that the particles are trapped far away from the surfaces can be found by observing the particles speeds. The velocity of particles being released from the traps (e.g. turning off the trapping laser) is much higher than the one of particles flowing at the bottom of the channel. This indicates that the traps are located closer to the intermediate plane in the channel, where the parabolic flow velocity profile generates higher

#80805 - $15.00 USD Received 8 Mar 2007; revised 25 Apr 2007; accepted 27 Apr 2007; published 2 May 2007

flow speeds.

4.2. Trapping efficiency

The maximal transverse trapping force F_r^{max} achievable with the micromirror tweezers was measured by the conventional viscous drag-force method relying on the Stokes formula. The force is reported using the normalized efficiency factor Q_r^{max} [25]

$$Q_r^{max} = \frac{cF_r^{max}}{n_{fluid}P_{trap}} = \frac{c(6\pi\eta a v_{max})}{n_{fluid}P_{trap}} \tag{4}$$

where n_{fluid} and η are respectively the fluid refractive index and dynamic viscosity, a is the particle radius, P_{trap} is the optical power available at the trap, and v_{max} is the maximal flow velocity that the trapped beads can sustain. Practically, the flow velocity in the fluidic channel was gently increased until the trapped particle escaped the trap, and the particle speed v_{max} after the escape was measured by video microscopy. Since the trapping efficiency measurements were performed close to the center of the micromirror array, the laser power at the trap is approximated by the peak irradiance I_0 of the trapping gaussian laser beam (of half width w and total power P_{tot}) incident onto the micromirror array, multiplied by the micromirror cross-section A (d is the diameter of the micromirror)

$$P_{trap} = \alpha I_0 A = \alpha \frac{P_{tot}}{2}\left(\frac{d}{w}\right)^2 \tag{5}$$

The factor α takes into account power losses, which are assumed to be restricted to the limited reflection at the golden mirrors (98.6%) and to residual reflections at the air-glass and the glass-water interfaces ($\alpha = 0.93$). Using a total laser power of $P_{tot} = 8W$, the central trap in the array receives a power of $P_{trap} = 34mW$. An escape velocity of $v_{max} = 385 \pm 62\mu m/s$ $(N = 20)$ was measured for the $9.33\mu m$ polystyrene beads, corresponding to a transverse trapping efficiency of $Q_r^{max} = 0.22 \pm 0.03$. The escape velocity measurements were performed on 20 different micromirrors, half of the measurements in a reverse flow direction to exclude asymmetry effects related to an eventual slight misalignment. These measurements were realized with an array of micromirrors whose focal plane was located relatively deep in the fluidic channel, $h \simeq 30 - 40\mu m$. This ensured that the particles were trapped far enough from the surface to limit proximity hydrodynamic force effects to less than 10% [26]. Also, the axial flow velocity gradient related to the parabolic flow velocity profile, which is not considered by the Stokes formula for the viscous force, is less pronounced closer to the central plane in the channel.

4.3. Multiple trapping associated with fluorescence light collection through the micromirrors

Due to the relatively large pitch of the present micromirror array ($250\mu m$) and the limited field-of-view of the microscope objective only a fraction of the trapping area could be viewed directly in the transmission mode with sufficient resolution for observing individual particles. Nevertheless, direct observation of the trapping area is not the only possibility, and might not even be necessary. The high-NA of the micromirrors allows surveying all particles in the array in a reflection mode, overcoming this field-of-view restriction. In order to demonstrate this possibility, the micromirrors were tested as fluorescence light collectors. A solution containing a mixture of fluorescent beads, $6\mu m$ in diameter (Molecular Probes AlignFlow), was let flow into the fluidic system. As particles are trapped at the focus of the micromirrors, they are simultaneously illuminated by the He-Ne fluorescence excitation lasers and emit fluorescent light. The latter is efficiently collected at high-NA by the micromirrors and sent through a 4-f system to the color camera (CCD2). The sequence in Fig. 6 illustrates the array of micromirrors "turning-

#80805 - $15.00 USD Received 8 Mar 2007; revised 25 Apr 2007; accepted 27 Apr 2007; published 2 May 2007

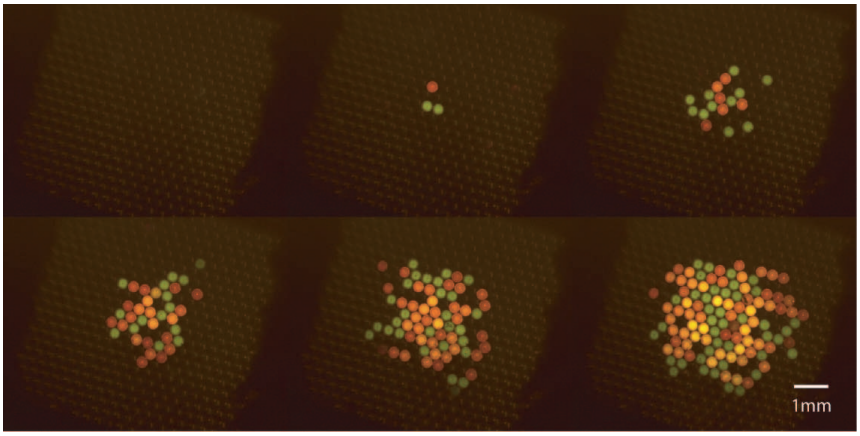

Fig. 6. (Movie 899KB) Sequence showing fluorescence light detection using the micromirrors. The colored circles are not the particles themselves, but the micromirrors "turning-on" as particles progressively fill the traps. The fluorescence light emitted by the trapped particles is collected with high-NA by the mirrors, and relayed onto the color camera though a 4-f system.

on" during the filling of the array, revealing the particle's individual fluorescence light color. Because of the gaussian profile of the trapping beam, the traps at the center of the array dispose of more optical power, thus particles can be trapped at higher flow speeds. No fluorescence signals could be observed from non-trapped particles at the CCD integration times ($50ms$) used in the present experiments.

5. Discussion

The physical configuration of the optical tweezers generated by the miniaturized parabolic mirrors is similar to that generated using a high-NA microscope objective, as both are single-beam gradient force optical traps. An advantageous difference consists in that high-NA parabolic mirrors produce convergent beams having proportionally more energy in the high spatial frequency components, due to their different apodization factor [27]. Peripheral rays in the converging cone of light are known to be of fundamental importance for the axial trap stability [28, 29], and also play an important role in the trap stability in the transverse direction [30]. Therefore, at equal NA, a parabolic mirror may allow generating more efficient traps than a high-NA objective lens. The transverse trapping efficiency of $Q_r^{max} \simeq 0.22$ obtained so far with the micromirrors is somewhat lower than typical reported values of $Q^{max} \simeq 0.25-0.35$ (for "large" $\sim 10\mu m$ polystyrene beads) using high-NA objective lenses [31, 23]. Such a relatively limited trapping efficiency may partially be explained by the micromirrors lower numerical aperture ($NA = 0.96$ with respect to commonly employed oil-immersion objective lenses performing $NA = 1.3$). Also, the micromirror surface quality has not been investigated yet, and may be inferior to that of the master microlens array due to non-conformities associated with the replication process. Finally, the spherical aberration caused by the refractive index interface at a trapping depth of $h \simeq 30-40\mu m$ may also be involved in this reduced efficiency [23]. Still, micromirrors could be designed to reach the same NAs as objective lenses, and their cross-sectional profile may be adapted to minimize aberration at a particular trapping depth.

A well-known issue related to the use of focusing mirrors, particularly if characterized by high-NA, is that slight deviations of the incident beam from the optical axis give rise to important levels of coma. Alignment accuracy should be better than 0.006^o to ensure undistorted

#80805 - $15.00 USD Received 8 Mar 2007; revised 25 Apr 2007; accepted 27 Apr 2007; published 2 May 2007

focusing [27]. Experimentally, it was observed that trapping was not as sensitive as this to the accurate alignment of the laser beam onto the micromirror array. Such a low sensitivity to alignment accuracy may be related to the miniature size of the mirrors, as the wavefront aberration scales with the size of the mirrors. Also, the sensitivity of the trapping efficiency to alignment was less important when handling relatively large particles ($9.33\mu m$ beads) than with the smaller $2.5\mu m$ particles closer in size to the wavelength.

The trap depth h above the cover-glass turned out to be a critical parameter for the efficient capture of particles in the fluidic device. As particles flow through the fluidic channel, they sediment and already flow in vicinity of the bottom of the channel when arriving at the trapping area. Therefore, the best catching yields were achieved with traps positioned 15 to $25\mu m$ above the bottom of the channel, ensuring that the particles were flowing in vicinity of the plane of the foci. Employing micromirror arrays with $h > 30\mu m$, particles could not be captured efficiently from the flowing solution unless operating at reduced flow speeds, allowing them enough time to raise to the level of the traps under the effect of the levitating radiation pressure.

The micromirror arrays used in these first experiments have a relatively large pitch of $250\mu m$, consequently limiting the trap density to the order of 20 traps$/mm^2$. Such large micromirrors were used only because microlens arrays having a smaller lens diameter, a parabolic profile and a sufficiently high NA were not commercially available. Employing smaller micromirrors would increase the trapping density inversely proportional to the square of the mirror size. Reasonably, micromirrors with a cross-sectional diameter smaller than $50\mu m$ may be used for trapping living cells, thus the trap density could reach 500 traps$/mm^2$. This is still by far below the highest optical trapping densities that have been achieved. However, as the trapping area is not restricted by the field of view of a microscope objective lens, the total number of traps may be increased at will (scalability). This advantage is essential when working with larger particles like living cells, having typical diameters in the $10-15\mu m$ range, as no more than 20-30 may be trapped simultaneously within the field of view of a high-NA objective lens. Trapping with micromirror arrays would allow increasing the total number of trapped cells by several folds. Micromirrors uniquely combine scalability with three-dimensional trapping, the latter certainly being an asset for working with biological particles having a large tendency to stick to the fluidic walls.

Another important advantage of the micromirror traps is their optical power throughput: they work with minimal power losses, when compared to tweezers based on microscope objective lenses wasting almost half of the laser power due to beam clipping or to limited optical transmission. Micromirrors also are achromatic, allowing undisturbed operation with different fluorescence wavelengths.

Obviously, trapping a large number of particles is not a goal by itself. Multiple optical trapping systems are very likely to find their highest potential in spectroscopic techniques, e.g. fluorescence or Raman spectroscopy [32], aiming at analyzing many particles at the same time and over extended periods of time. For such applications the ability to efficiently detect individual light signals from all the trapped particles at the same time is of primary importance. As demonstrated in the first experiments with artificial fluorescent particles reported above, micromirror trap arrays can be used to collect individual light signals at high-NA simultaneously from all trapped particles, giving access to multi-particle high sensitivity levels of detection. Very large assemblies of living cells could be achieved using micro-mirror arrays, opening the way for massively parallel analysis. Statistically relevant data may be collected within a single experiment, avoiding time-consuming repetitive experiments and ensuring that all particles are analyzed in the same experimental conditions.

Micromirror arrays may advantageously be integrated in microfluidic systems. In the present study, a simple fluidic device was developed only for the purpose of demonstrating the mi-

#80805 - $15.00 USD Received 8 Mar 2007; revised 25 Apr 2007; accepted 27 Apr 2007; published 2 May 2007

cromirror's trapping and fluorescence light collection possibilities. More sophisticated devices combining microoptics and microfluidics have been described [33]. Micromirrors may very simply be integrated in similar systems, and are potentially inexpensive and mass producible, e.g. using mold casting techniques. They are ideal candidates for optical traps integrated in lab-on-a-chip type microflow devices.

6. Conclusions

Multiple 3D optical trapping using parabolic micromirror arrays has been demonstrated. The trapping performances of these optical tweezers are comparable to those of conventional tweezers relying on macroscopic optical components. The micromirror approach allows multiple trapping in a highly scalable approach: every trap possesses its own miniaturized focusing element, thus the total number of traps is not restricted as in schemes relying on high-NA microscope objectives having a very limited field-of-view. Simultaneous yet individual fluorescence detection from all trapped particles is demonstrated using the micromirrors as high-NA light collectors, thus opening the way for multi-particle high-sensitivity levels of detection. Micromirrors could easily be integrated into all kinds of micro-fluidic systems. They represent an ideal solution for miniaturized multiple optical traps in lab-on-a-chip devices.

Acknowledgements

This work was supported by the Swiss Innovation Promotion Agency (CTI TopNano21 Project No. 6983.1). The authors are grateful to Gerben Boer for his contributing knowledge in microoptics, and to Alexandre Perentes for his assistance with gold evaporation processes.

#80805 - $15.00 USD Received 8 Mar 2007; revised 25 Apr 2007; accepted 27 Apr 2007; published 2 May 2007